Photophysics of nanomaterials for opto-electronic applications

Kahmann, Simon

8 Trap States in Lead Sulphide Colloidal Quantum Dots

In this chapter, the low energy pump-probe set-up is employed to investigate photoinduced transitions of lead sulphide CQDs in the MIR spectral region with an unprecedentedly high resolution in energy. For a range of particle sizes and different surface ligands, the formation of two distinct absorption bands is observed. Supported by investigations of different surface treatments, these bands can be assigned to trap-to-band excitations from trap states within the band gap. This technique thus offers both additional basic insight into the properties of this material class, as well as being a viable tool for assessing the material quality.

8.1 Introduction

Colloidal quantum dots are an interesting class of materials for opto-electronic applications. As outlined in section 2.4.2, much of the progress in this field, especially for solar cells, has been achieved using lead sulphide. The successful introduction into efficient devices is generally accomplished by treatments of the CQD surface. Most prominently, the long insulating ligands, which promote their colloidal stability, need to be exchanged, to allow for proper charge carrier conduction (section 2.4.4). The modification of the surface, however, is prone to introducing states within the band gap, which can subsequently act as electronic traps and hamper the flow of charge carriers.[1] Indeed, the high surface to volume ratio renders the CQDs vulnerable to surface related defects, which might be caused by incomplete surface passivation, surface oxidation or interfacial states.

Such defect states were observed for PbS by various techniques. Reported was especially a state 0.2 eV above the valence level of 1,2-ethanedithiol or 1,3-mercaptopropionic acid (EDT, MPA) capped CQDs *via* Kelvin probe force microscopy (KPFM) and scanning tunnelling spectroscopy (STS).[2–5] Additionally, studies on transport phenomena reported a quasi-metallic mid-gap band

S. Kahmann, M. Sytnyk, N. Schrenker, G. J. Matt, E. Spiecker, W. Heiss, C. J. Brabec, M. A. Loi, Revealing Trap States in Lead Sulphide Colloidal Quantum Dots by Photoinduced Absorption Spectroscopy, *Adv. Electr. Mater.*, just accepted, doi:10.1002/aelm.201700348.
TEM micrographs were taken by Nadine Schrenker.

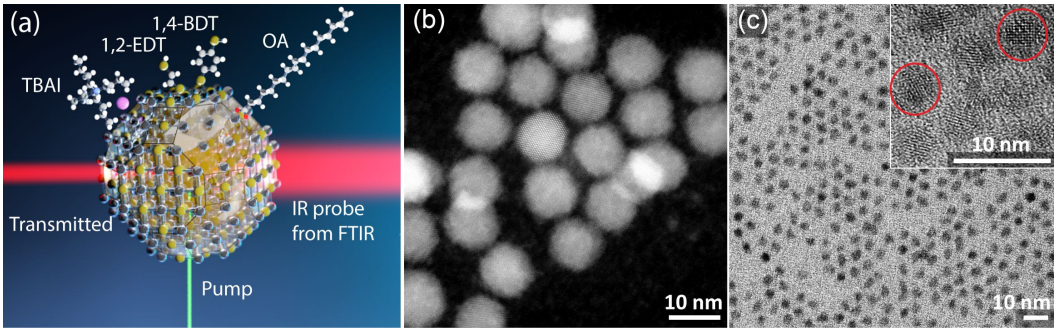

Figure 8.1: Sketch of the pump-probe measurement including the different ligands employed in this study (a). These include oleic acid (OA), 1,4-benzendithiol (BDT), 1,2-ethanedithiol (EDT) and tetrabutylammonium iodite (TBAI). The HRSTEM image of large (b) and HRTEM image of small CQDs with a magnification in its inset (c) show the highly regular shape of the as-synthesised material.

approximately 0.4 eV below the conduction level of EDT capped PbS.[6,7] Furthermore, a trap distribution with an activation energy of 0.34 eV was found using impedance spectroscopy for PbS treated with tetrabutylammonium iodite (TBAI).[8]

Moreover, using optical pump-probe spectroscopy, a broad photoinduced absorption around 0.3 eV was observed for a range of ligands, including EDT and MPA.[9,10] This feature was assigned to trap-to-band transitions. With a combination of optical pump and electrical probe spectroscopy on EDT and MPA capped PbS, two independent trap distributions, were also reported.[11]

The corruption of the clean band gap through ligand exchange was furthermore related to the emergence of photoluminescence signals at energy below the direct band gap transition.[12–14] Indeed, the latter reports underlined that these states lead to a significant reduction in open circuit voltage and thereby overall solar cell efficiency.[15] A clear understanding of these in-gap states, and how to suppress them, is thus crucial for further improvement of these materials for future applications.

8.2 Results and discussion

CQDs were investigated when covered with their native OA or with shorter entities commonly used in device fabrication, namely 1,4-benzenedithiol (BDT), EDT and TBAI. Their respective molecular structure is depicted in Figure 8.1 (a), alongside the measurement principle. Three batches of differently sized CQDs were examined: *small* with a first excitonic peak at 1.24 eV, *medium* at 1.11 eV and *large* at 0.76 eV, as shown Figure 8.2 (a) (measured in toluene). The approximate size range can be inferred from the position of the excitonic peak (Figure 2.21), but to more precisely determine their size and their shape, high resolution electron microscopy (HRSTEM and HRTEM) images were acquired (Figure 8.1 (b) and (c)). The large particles in (b) exhi-

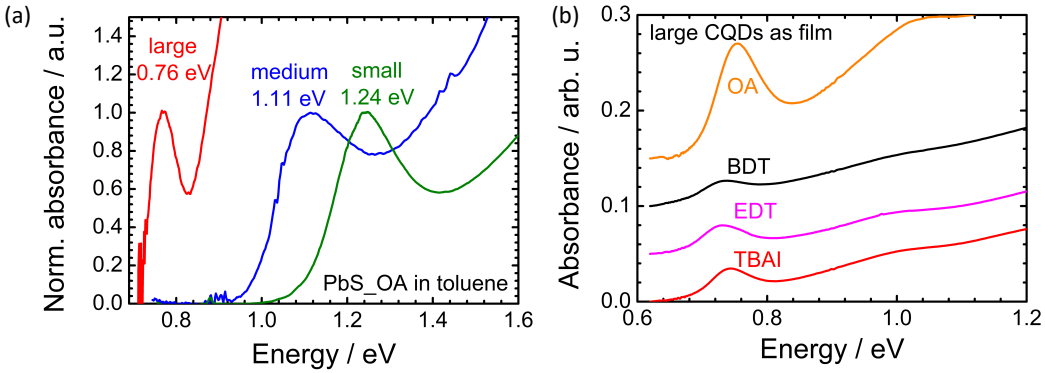

Figure 8.2: Normalised absorbance spectra of the employed CQDs in toluene solution (a) with their position of the first excitonic peak denoted. Absorbance of large particles with the respective ligands when cast as a film on glass (b).

bit a highly regular shape with a mean particle size of 10.6 nm, as determined from selected area diffraction (SAD, not shown). The small particles (4.2 nm; Figure 8.1 (c)) similarly exhibit a regular shape, with clearly discernible crystal planes, as depicted in the inset. The quantum confinement is retained in cast films, also after ligand exchange, as can be inferred from the pronounced excitonic peak in the absorption spectra in Figure 8.2 (b).

Since all spectral features were determined to be independent of the excitation energy, only spectra for 1.6 eV (780 nm) excitation are depicted in the following.
Figure 8.3 summarises the results for small, medium and large PbS CQDs, when covered with the different ligands. Each spectrum displays a broad region of photoinduced absorption below 0.5 eV consisting of two clearly resolvable, but overlapping bands. These bands shift significantly from approximately 0.2 and 0.4 eV, for small CQDs, down to 0.1-0.2 eV, for large CQDs. For a larger band gap, the PIA bands are hence found at larger energy (also consider Figure 8.3 (d)). Some of the samples exhibit narrow features superimposed on the broad bands, which will be discussed separately below.
Comparing the different ligands for the same particle size, one finds that the formation of two distinct bands is common to all investigated samples and no additional signals arise or vanish upon ligand variation. All curves were thus fitted using two Gaussian peaks, leading to the peak energies indicated in Figure 8.3 (d) and presented in Table A4. Interestingly, large CQDs exhibit narrower distributions, which correlates with their narrower absorption spectra, as seen in Figure 8.2. The same is true for TBAI treated PbS. Small variations in PIA shape and position are thus not due to the capping ligands themselves (*i.e.* their chemical nature), but are assigned to changes in confinement, *i.e.* the average band gap energy and variance thereof. As can furthermore be seen from the increasing separation of the two peaks for larger band gap CQDs (Figure 8.3 (d)), the transition energies scale differently with size, making a shared origin unlikely.

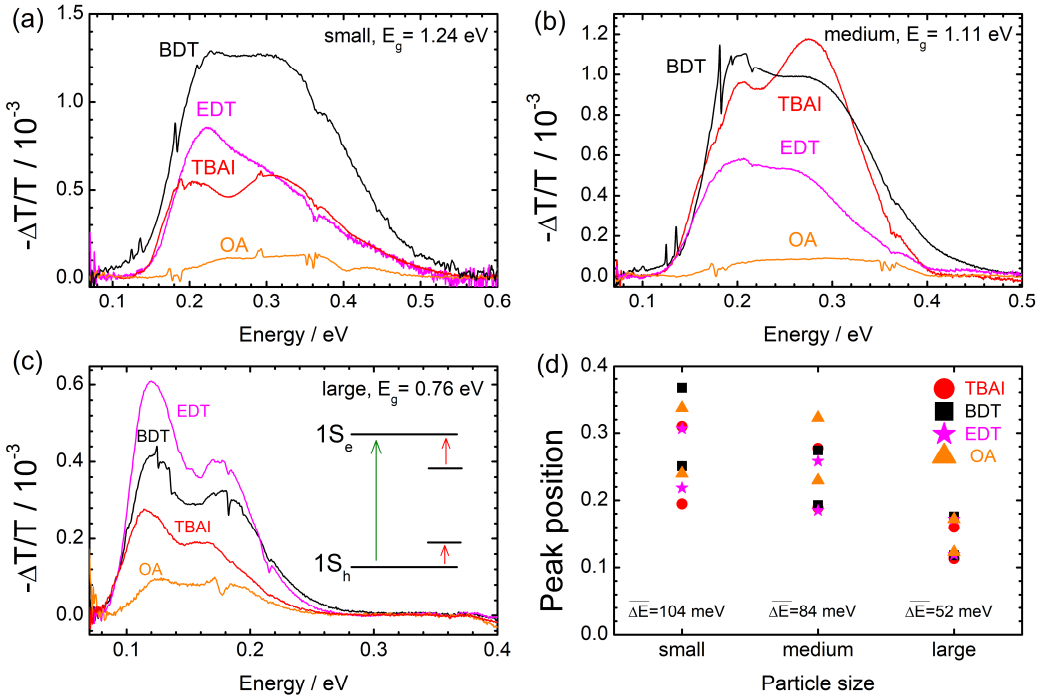

Figure 8.3: PIA spectra of films of small (a), medium (b) and large (c) CQDs capped with different ligands (1.6 eV excitation). Peak positions for each spectrum and their average separation are summarised in (d). The sketch in the inset of (c) depicts the excitation of the CQD in green and the proposed re-excitation of trapped carriers in red.

Photoinduced transitions in this energy region may be explained by higher excitations from already excited CQDs,[16] *e.g.* lifting an electron from the $1S_e$ to the $2P_e$ level. For excitons, this would lead to a small signal in a steady-state measurement and generally to an increased signal for CQDs with larger exciton lifetime (τ(PbS_OA) > τ(PbS_BDT), Chapter 7). It can therefore be dismissed as origin for the PIA bands. More probably, the PIA could be due to higher excitations of free carriers, formed after exciton dissociation (intraband transitions), as they exhibit a significantly longer lifetime.

As will be discussed in the following, the origin is more likely to involve carriers trapped in surface states. These allow for trap-to-band transitions as depicted in the inset of Figure 8.3 (c). As the magnitude of the signal is strongly governed by the capping ligands, this confirms the view of ligands to work as passivating agents. In this picture, the well passivating native OA suppresses the formation of trap states and exchanging it leads to an increased density of traps. Consequently, an increased PL emission at energy lower than the band gap value can be observed for ligand-exchanged CQDs (Figure 8.4), especially for EDT and TBAI treated samples, which has previously been assigned to trap induced emission.[12–14] Furthermore notable, the PIA signal strength drastically decreases for large CQDs (Figure 8.3). This trend is not explainable for in-

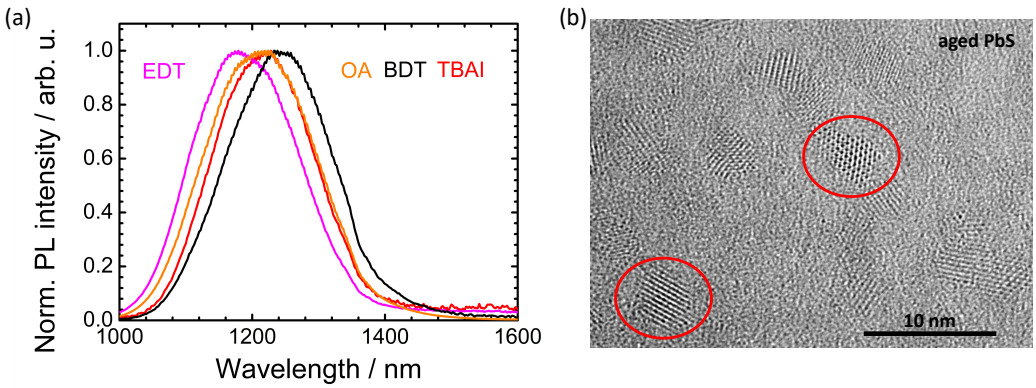

Figure 8.4: Steady state PL of PbS CQDs for different ligands (a) depicting a significant below band gap emission after ligand exchange (inset). The HRTEM image of degraded particles displays a pronounced surface reconstruction whilst the crystalline cores are retained.

traband transitions. Fewer defects due to the lower surface to volume ratio of large CQDs, in contrast, readily explain this behaviour.

To further elucidate the origin of these states, CQDs covered with native OA were investigated in further detail. As reported in Figure 8.3, the PIA for these CQDs is significantly lower than for the exchanged ones, but the absorption bands are still present. First, the impact of degradation was monitored by storing a sample of small CQDs for one year under air at room temperature and exposed to sun light. The HRTEM image in Figure 8.4 (b) displays a dramatically reconstructed surface and the irregular shape of these CQDs. The comparison with the fresh material in Figure 8.5 (a) reveals a drastically increased signal and more pronounced narrow features. Again, intraband transitions cannot explain this trend and trap states are convincing candidates for such behaviour. While air exposure, leading to oxygen adsorption and trap state generation was reported before, [3] it was also pointed out that the adsorption was reversible under vacuum. Given the extended storage under vacuum, immediately prior to the measurement (at least 12 h), the amount of adsorbed oxygen in these experiments should therefore be negligible.
A more probable explanation for the increased signal would be the removal of surface ligands and surface reconstruction upon environmental exposure. Besides atom reorientation, which is evident from the HRTEM image in Figure 8.4, the degree of ligand coverage is also likely to change upon environmental exposure.

This effect on the PIA spectra of small PbS_OA was subsequently investigated by varying the post-synthesis washing as a way to remove capping ligands. Strikingly, as displayed in Figure 8.5 (b), as-synthesised (unwashed) CQDs do not exhibit any absorption at 0.36 eV. Only the lower energy absorption band is weakly present for this sample. For the "normal" washing protocol (four cycles after synthesis, consider method section 8.4) and extensive washing (eleven cycles), both absorption bands are present and the signal strength increases with the number of washing

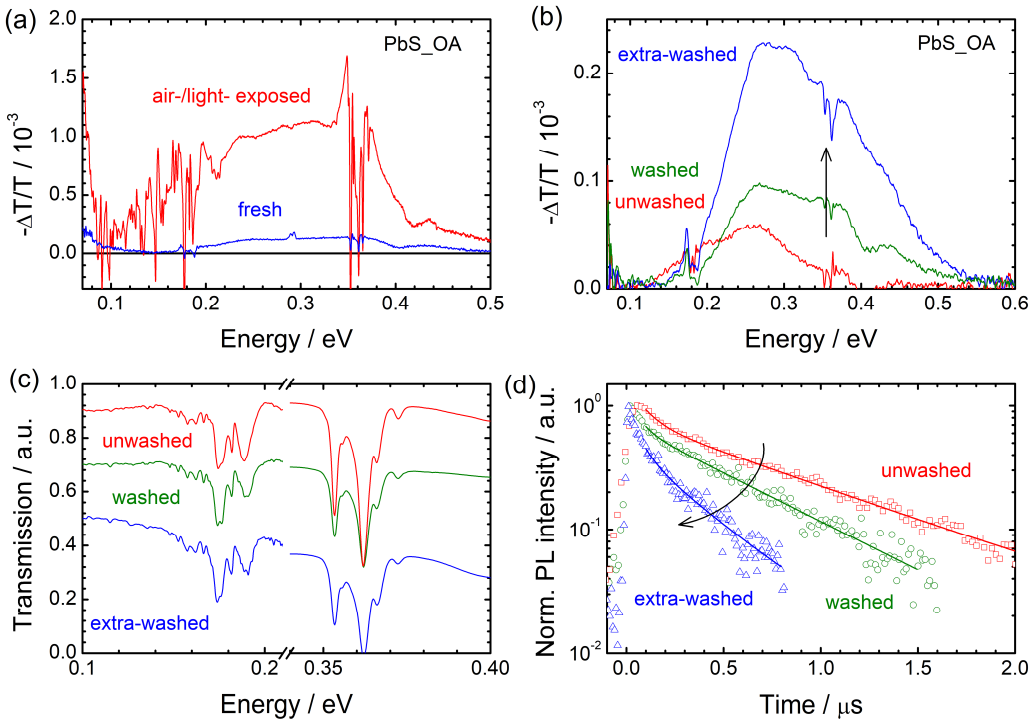

Figure 8.5: PIA spectra of freshly prepared *versus* air exposed PbS_OA (a) and after different degrees of washing (b). Degradation and extensive washing increase the PIA response. As-synthesised CQDs do not exhibit a signal at 0.36 eV. The corresponding MIR transmission does not offer changes in surface chemistry (c), but the PL lifetime decreases upon washing (d).

steps. This trend agrees well with previous observations of a decreasing J_{SC} in CQD solar cells upon excessive post-synthesis washing, which was related to trap mediated recombination. [17] Importantly, the surface chemistry of OA ligands does not change upon washing (consider normalised transmission spectra in (c)), whereby chemical modification during the washing procedure can be excluded. Underlining this trend, also the transient PL, depicted in (d), exhibits a lifetime reduction upon increased washing, which can be predominantly attributed to a larger concentration of trap states.

Concluding the first part of this investigation, two separate trap states in the band gap of PbS CQDs are found, which shift towards higher energy for CQDs of larger band gap. These bands are located in the energy region previously associated with trap states. The observation of two distinct distributions may explain why some groups reported states close to the valence level and others associated them with the conduction level. [2–7,18]

The surface chemistry of PbS CQDs is more complex than simple schemes such as the one in Figure 8.1 (a) suggest. Even as-synthesised CQDs do not only exhibit two differently polarised crystal facets ((001) and (111), section 2.4.4), but are also covered with hydroxyl and oleate ions,

additional to oleic acid. [19] Kim *et al.* furthermore suggested that besides to defects, in-gap states were related to the overall stoichiometry of the CQD surface. [1] It is thus likely that washing and the concomitant stripping of ligands not only leads to a change in degree of surface coverage, but also of surface composition. This, in turn, affects the partial charges of Pb and S atoms on the CQD surface and generates the in-gap trap states. Especially the energy region around 0.37 eV (for small particles) was previously linked to elemental Pb^0 in CQDs. [20] Similarly, the exposure to oxygen was proposed to lead to a remodelling of the surface structure and change of the local Pb:S ratio. [21] In this light, it seems plausible that a prolonged exposure to air leads to an extended surface remodelling as observed in Figure 8.4, which in turn leads to a stronger PIA signal.
Further theoretical studies focusing on the impact of the Pb and S oxidation states seem thus to be a promising route to a deeper understanding of the trap formation.

In the following, the narrow features superimposed on the broad PIA bands will be discussed. Notably, these are only observable for OA and BDT capped CQDs. Narrow features in this region were reported before, but not further analysed. [9,10]
To allow for a proper comparison, the low energy transmission spectra of pristine OA, PbS_OA and the corresponding PIA spectrum for medium and large particles are depicted in Figure 8.6 (a). As stated above, OA partially deprotonates to bind as oleate (OA^-) to surface Pb^{2+} on the polar (111) facet and OA bidentately bridges Pb and S atoms on the (001) facet. [10,19] The deprotonation of OA is apparent by the emergence of two broad absorption bands around 0.185 eV (1500 cm^{-1}) in Figure 8.6 (a), which are due to the symmetric and asymmetric stretch vibrations of the anchoring carboxyl-group (Table A5). In the PIA spectra, narrow features are observable both in the region of mehtyl- and methylene (CH_x) vibrations, slightly below 0.36 eV (3000 cm^{-1}) and for the COO^- vibrations around 0.185 eV. Strikingly, however, the carboxyl features are only observable for the medium sized (and small) CQDs, where the features energetically coincide with the trap induced PIA band.

In case of BDT, as depicted in 8.6 (b), most of the features of unattached ligands coincide with those of PbS_BDT, but some absorption lines are significantly weaker for the latter (also consider Table A6). This is especially the case for those at 0.1 and 0.17 eV (800 and 1380 cm^{-1}). Although the BDT molecule is assumed to remain chemically unchanged upon binding to PbS CQDs, the attachment can change dipole moments in the environment and reduce the molecule's symmetry. As a consequence, oscillator strengths and resonant energies may change. Figure 8.6 (b) shows that also for BDT all narrow features in the PIA spectrum coincide perfectly with molecular vibrations observed in transmission. The shape of these features, however, is drastically different for the two particle sizes (at the same energy) and also varies for the same size (at different energies).

Such features could, in principle, be caused by the Stark effect, *i.e.* by the electrical field of

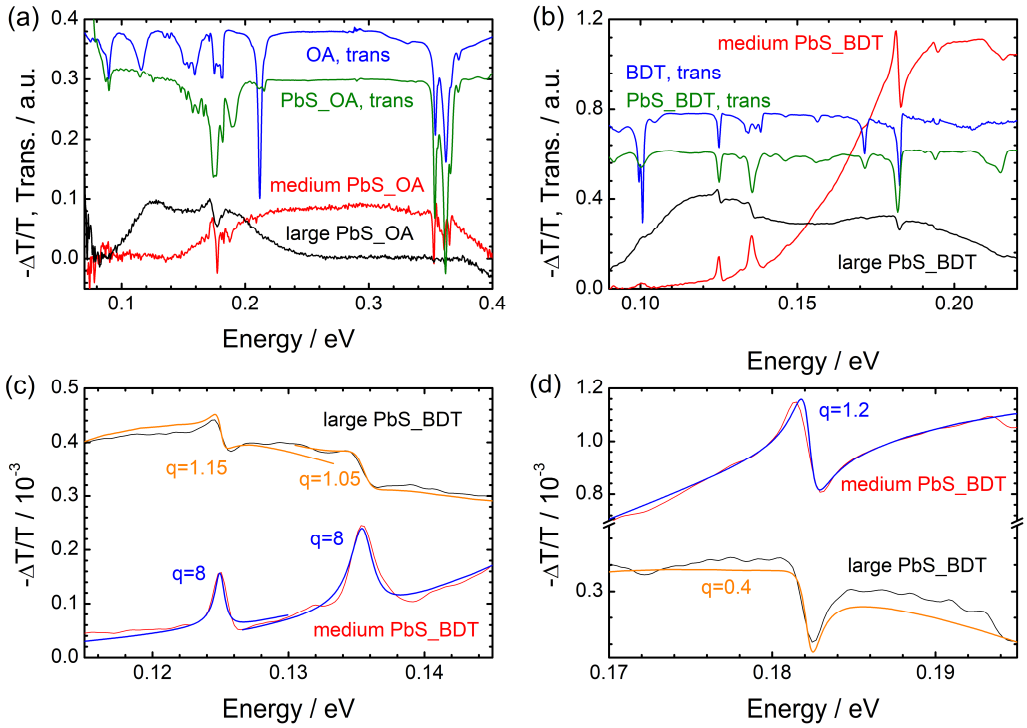

Figure 8.6: Transmission spectra of neat OA (a) and BDT (b) and when capping PbS CQDs along with the PIA spectra for small and medium PbS. Close-up of the low energy region of the PbS_BDT PIA spectra with Fano profiles fitted to the pronounced narrow features (c), (d).

trapped charges acting on the resonant frequency of the molecular vibrations of attached ligands. The Stark effect, however, fails to explain why for PbS_BDT the shape of the narrow features changes for different particle sizes and why PbS_OA only exhibits narrow features for small CQDs.

In contrast, these features are readily explainable as Fano resonances.[22] In order for this effect to occur, a narrow vibration needs to interact with an energetically broad process coinciding in energy. The resulting Fano profile has the form of

$$FP = \frac{(\epsilon + q)^2}{\epsilon^2 + 1}, \tag{8.1}$$

where q is a phenomenological shape parameter and ϵ is the reduced energy defined as $\epsilon = (2(E - E_{FR})/\Gamma)$. E_{FR} is the resonant energy of the Fano process, E the energy and Γ is the width of the narrow vibration.

Using this profile, the three most pronounced narrow features for PbS_BDT between 0.12 and 0.19 eV were modelled. As depicted in Figure 8.6 (c) and (d), this model yields a remarkable agreement with the experimental data. As indicated, the q-parameter employed is large when

the molecular vibration and the peak of the trap distribution are widely separated and approaches zero when they almost coincide. This fits the interpretation of q as a measure for their interaction. In case of a large q, this is weak. When q is around 1, the continuum transition and the narrow vibration are of the same strength.
Accordingly, the absence of narrow features around 0.36 eV for large PbS_OA is a consequence of the absence of a continuous state at that energy.
However, to precisely understand why only some of the vibrations lead to features in the PIA spectra is beyond the scope of this work. A more thorough understanding of the mechanisms, however, will ultimately offer more fundamental insight into the nature of ligand binding to surface atoms. Notably, all of the PbS_BDT PIA signals are related to the benzene ring vibrations and none to the anchoring -SH group (Table A6). Accordingly, no narrow features can be observed for PbS_EDT, despite a rich spectrum of molecular vibrations characterising EDT.

8.3 Conclusion

In conclusion, mid infrared photoinduced absorption spectra of lead sulphide CQDs capped with ligands commonly applied for (opto-)electronic applications were studied. Two distinct PIA bands were observed to form and ascribed to surface trap states. While these two bands shift from approximately 0.35 and 0.22 eV for CQDs with a first excitonic peak around 1.2 eV towards energies between 0.1 and 0.2 eV for large diameter particles with an excitonic peak around 0.8 eV, their position is not affected by the type of ligand attached to the surface. The energy region spans all values so far linked to trap- or in-gap states of PbS CQDs in the literature. The variations found in literature are therefore assigned to be due to the investigation of CQDs of different size. The magnitude of the photoinduced bands changes upon exchanging the native oleic acid to shorter ligands. Similarly, extensive exposure to light and air do not affect the spectral features other than by increasing their intensity. These traps are thus associated with the atoms inherent in the surface of the CQDs rather than interface states caused by the binding of surface ligands. For CQDs covered with BDT or OA, narrow features are additionally observed in the PIA spectra, which can be connected to the ligands' molecular vibrations. Their emergence is explained as Fano resonances occurring between molecular vibrations and the continuous trap bands.
The PIA technique employed herein is hence a viable tool for assessing the quality of the surface passivation of CQDs – a crucial aspect for further optimisation of future device performance.

8.4 Methods

Synthesis: CQDs were synthesised as reported before.[23] Briefly, PbO was dissolved in a OA/ODE mixture under vacuum at 130 °C for 1 h. The sulphur precursor was prepared trough dissolving HMDT in dried ODE, which was then rapidly injected into vigorously stirring lead oleate under argon (Pb/S molar ratio was 2:1.7) at 150 °C. After self-cooling of the mixture down to room temperature, ODE was added followed by washing steps, which were carried out *via* precipitation with anhydrous ethanol, centrifugation at 8000 rpm and re-dispersion in anhydrous n-hexane. The CQDs are eventually dissolved in anhydrous toluene. From 4 to 11 washing steps were carried out.

TEM analysis: For TEM analysis, the PbS nanoparticle solution was coated onto a thin carbon film. HRTEM and HRSTEM images of large and of aged particles were taken at a double-corrected FEI Titan Themis^3 300 at 200kV. Selected area diffraction patterns (SAD) were taken at a Philips CM300 UT at 300kV. The mean nanoparticle size was determined from the diffraction patterns by applying the Scherrer equation using a shape factor of K=0.89 for spheres. The images for fresh small particles were obtained using a JEOL 2011 FasTEM microscope operating at an acceleration voltage of 200 kV.

Sample preparation: Thin films were spin-cast from solution on ZnSe platelets in a layer-by-layer fashion. The ligand treatment included soaking the cast layer for 1 min in the ligand-to be (BDT: 2.8 mg/ml in MeCN, EDT: 0.01 vol-% in MeCN, TBAI: 10 mg/mL in MeOH) with an additional cleaning step using the neat solvent.

PIA measurement: The substrates were subsequently mounted into a cryostat without having been exposed to air (if not stated otherwise). To avoid perturbations from the pump light, a GaAs filter was placed in front of the detector. Spectra were acquired with a resolution of 5 cm^{-1} and the measurement cycle was run at least 1024 times. The "light off" spectrum was also used as transmission measurement.

Photoluminescence: The respective films were deposited on quartz substrates, mounted in a nitrogen filled sample holder and excited at 400 nm using the second harmonic of the mode-locked Ti:sapphire laser.

Bibliography

[1] D. Kim, D.-H. Kim, J.-H. Lee, J. C. Grossman, Impact of Stoichiometry on the Electronic Structure of PbS Quantum Dots, *Phys. Rev. Lett.* 110, 196802 (2013).

[2] Y. Zhang, D. Zherebetskyy, N. D. Bronstein, S. Barja, L. Lichtenstein, D. Schuppisser, L.-w. Wang, A. P. Alivisatos, M. Salmeron, Charge Percolation Pathways Guided by Defects in Quantum Dot Solids, *Nano Lett.* 15, 3249 (2015).

[3] Y. Zhang, Q. Chen, A. P. Alivisatos, M. Salmeron, Dynamic Charge Carrier Trapping in Quantum Dot Field Effect Transistors, *Nano Lett.* 15, 4657 (2015).

[4] Y. Zhang, D. Zherebetskyy, N. D. Bronstein, S. Barja, L. Lichtenstein, A. P. Alivisatos, L.-W. W. Wang, M. Salmeron, Molecular Oxygen Induced in-Gap States in PbS Quantum Dots, *ACS Nano* 9, 10445 (2015).

[5] B. Diaconescu, L. A. Padilha, P. Nagpal, B. S. Swartzentruber, V. I. Klimov, Measurement of Electronic States of PbS Nanocrystal Quantum Dots Using Scanning Tunneling Spectroscopy: The Role of Parity Selection Rules in Optical Absorption, *Phys. Rev. Lett.* 110, 1 (2013).

[6] P. Nagpal, V. I. Klimov, Role of Mid-Gap States in Charge Transport and Photoconductivity in Semiconductor Nanocrystal Films, *Nat. Commun.* 2, 486 (2011).

[7] D. Bozyigit, S. Volk, O. Yarema, V. Wood, Quantification of deep traps in nanocrystal solids, their electronic properties, and their influence on device behavior - SI, *Nano Lett.* 13, 5284 (2013).

[8] Z. Jin, A. Wang, Q. Zhou, Y. Wang, J. Wang, Detecting trap states in planar PbS colloidal quantum dot solar cells, *Sci. Rep.* 6, 37106 (2016).

[9] K. S. Jeong, J. Tang, H. Liu, J. Kim, A. W. Schaefer, K. Kemp, L. Levina, X. Wang, S. Hoogland, R. Debnath, L. Brzozowski, E. H. Sargent, J. B. Asbury, Enhanced Mobility-Lifetime Products in PbS Colloidal Quantum Dot Photovoltaics, *ACS Nano* 6, 89 (2012).

[10] J. Tang, K. W. Kemp, S. Hoogland, K. S. Jeong, H. Liu, L. Levina, M. Furukawa, X. Wang, R. Debnath, D. Cha, K. W. Chou, A. Fischer, A. Amassian, J. B. Asbury, E. H. Sargent, Colloidal-Quantum-Dot Photovoltaics Using Atomic-Ligand Passivation., *Nat. Mater.* 10, 765 (2011).

[11] A. A. Bakulin, S. Neutzner, H. J. Bakker, L. Ottaviani, D. Barakel, Z. Chen, Q. Dot, P. Devices, A. A. Bakulin, S. Neutzner, H. J. Bakker, L. Ottaviani, Charge Trapping Dynamics in PbS Colloidal Quantum Dot Photovoltaic Devices, *ACS Nano* 7, 8771 (2013).

[12] G. W. Hwang, D. Kim, J. M. Cordero, M. W. B. Wilson, C.-H. H. M. Chuang, J. C. Grossman, M. G. Bawendi, Identifying and Eliminating Emissive Sub-bandgap States in Thin Films of PbS Nanocrystals, *Adv. Mater.* 27, 4481 (2015).

[13] M. J. Speirs, D. N. Dirin, M. Abdu-Aguye, D. M. Balazs, M. V. Kovalenko, M. A. Loi, Temperature dependent behaviour of lead sulfide quantum dot solar cells and films, *Energy Environ. Sci.* 9, 2916 (2016).

[14] C.-H. M. Chuang, A. Maurano, R. E. Brandt, G. W. Hwang, J. Jean, T. Buonassisi, V. Bulović, M. G. Bawendi, Open-Circuit Voltage Deficit, Radiative Sub-Bandgap States, and Prospects in Quantum Dot Solar Cells, *Nano Lett.* 15, 3286 (2015).

[15] M. J. Speirs, D. M. Balazs, H.-H. Fang, L.-H. Lai, L. Protesescu, M. V. Kovalenko, M. A. Loi, Origin of the increased open circuit voltage in PbSâĂŞCdS coreâĂŞshell quantum dot solar cells, *J. Mater. Chem. A* 3, 1450 (2015).

[16] B. L. Wehrenberg, C. Wang, P. Guyot-Sionnest, Interband and Intraband Optical Studies of PbSe Colloidal Quantum Dots, *J. Phys. Chem. B* 106, 10634 (2002).

[17] C. Piliego, L. Protesescu, S. Z. Bisri, M. V. Kovalenko, M. A. Loi, 5.2% efficient PbS nanocrystal Schottky solar cells, *Energy Environ. Sci.* 6, 3054 (2013).

[18] M. I. Nugraha, R. Häusermann, S. Z. Bisri, H. Matsui, M. Sytnyk, W. Heiss, J. Takeya, M. A. Loi, High mobility and low density of trap states in dual-solid-gated PbS nanocrystal field-effect transistors, *Adv. Mater.* 27, 2107 (2015).

[19] D. Zherebetskyy, M. Scheele, Y. Zhang, N. Bronstein, C. Thompson, D. Britt, M. Salmeron, P. Alivisatos, L.-W. Wang, Hydroxylation of the Surface of PbS Nanocrystals Passivated with Oleic Acid, *Science* 344, 1380 (2014).

[20] D. Zherebetskyy, Y. Zhang, M. Salmeron, L. W. Wang, Tolerance of Intrinsic Defects in PbS Quantum Dots, *J. Phys. Chem. Lett.* 6, 4711 (2015).

[21] F. Bertolotti, D. N. Dirin, M. Ibáñez, F. Krumeich, A. Cervellino, R. Frison, O. Voznyy, E. H. Sargent, M. V. Kovalenko, A. Guagliardi, N. Masciocchi, Crystal Symmetry Breaking and Vacancies in Colloidal Lead Chalcogenide Quantum Dots, *Nat. Mater.* 15, 987 (2016).

[22] U. Fano, Effects of configuration interaction on intensities and phase shifts, *Phys. Rev.* 124, 1866 (1961).

[23] M. A. M. Hines, G. G. D. Scholes, Colloidal PbS Nanocrystals with Size-Tunable Near-Infrared Emission: Observation of Post-Synthesis Self-Narrowing of the Particle Size Distribution, *Adv. Mater.* 15, 1844 (2003).